An Anisotropic and Asymmetric Causal Filtering Based Corner Detection Method

Ghulam Sakhi Shokouh, Philippe Montesinos, Baptiste Magnier

An Anisotropic and Asymmetric Causal Filtering Based Corner Detection Method

Ghulam Sakhi Shokouh[a], Philippe Montesinos[b] and Baptiste Magnier[c]
EuroMov Digital Health in Motion, Univ. Montpellier, IMT Mines Ales, Ales, France
{*ghulam-sakhi.shokouh, philippe.montesinos, baptiste.magnier*}*@mines-ales.fr*

Keywords: Causal filter, Anisotropic filtering, Asymmetric diffusion, Corner detection

Abstract: An asymmetric-anisotropic causal diffusion filtering-based curvature operator is proposed in this communication. The new corner operator produces optimal results on small structures, such as, corners at pixel level and also sub-pixel level precision. Meanwhile, this method is robust against noises due to its asymmetric diffusion scheme. Experiments have been performed on a set of both synthetic and real images. The obtained results are promising and better without any ambiguity as compared with the two referenced corner operators, namely Kitchen Rosenfeld and Harris corner detector.

1 INTRODUCTION

The importance and interest in keypoint detection (i.e, corner or junction as a stable interest point) in a digital image lies notably in its application in image matching, tracking, motion estimation, panoramic stitching, object recognition, and 3D reconstruction (Schmid et al., 2010). The reason for the corner detection's wide range of applications is that the corner is easier to localize than other low-level features such as edges or lines, particularly taking into consideration the correspondence problems (e.g., aperture problem in matching). There are many corner detection techniques based on classic handcrafted (Shokouh et al., 2023) and deep learning methods (Wang et al., 2019). Deep learning-based techniques are more automatic, however, considering the accuracy and precision for the detection of small structures, such as corners, keypoints, etc., they do not generally present higher performance (highly depends on the dataset quality, and annotation which is not easy for small structures). We argue that handcrafted techniques are still widely used, particularly for optimization purposes, either independently or integrated into the preprocessing or post-processing stages of machine learning based higher-level computer vision applications (Junfeng et al., 2022). One of the example of computer vision application that its performance directly depends on the precision and accuracy of keypoint detection is 3D reconstruction. Additionally, among the classic handcrafted corner detection techniques, the two corner detection operators Kitchen and Rosenfeld (Kitchen and Rosenfeld, 1982), and Harris (Harris and Stephens, 1988), are the main method used for the comparison and benchmarking. Moreover, Causal filtering has proven its efficiency in many segmentation domains, such as edge or line detection. In this contribution, we are presenting a new segmentation method for corner detection based on asymmetric anisotropic diffusion filtering. The basic idea is inspired from a curvature-like operator similar to the Kitchen-Rosenfeld operator, but implemented through an asymmetric diffusion scheme using an anisotropic causal filter. Finally, we have compared the experimental result of our operator with the Kitchen and Rosen- feld, and Harris, the visual result presented higher precision for both pixel level and sub-pixel level. The structure of this paper consists of related works in the subsequent section, followed by the proposed methods and the obtained result, and eventually, the conclusion is presented.

2 RELATED WORKS

Considering a curve traced on the image plane, the curvature is defined as $\frac{d\theta}{ds}$ where θ is the tangent to the curve and s the curvilinear coordinate along the curve. As an image, $I(x,\ y)$ is a Cartesian parametrized sur-

[a] https://orcid.org/0000−0003−2561−7317
[b] https://orcid.org/0000−0003−3741−8702
[c] https://orcid.org/0000−0003−3458−0552

face as Eq. 1:

$$z = I(xy) \tag{1}$$

An image can then be considered also as a set of isophotes lines, at each pixel, there is in isophote line going through this pixel. We can then define the dense (at each pixel) the curvature of isophote lines in an image is Eq. 2:

$$\frac{d\theta}{ds} = \frac{I_y^2 I_{xx} - 2I_x I_y I_{xy} + I_x^2 I_{yy}}{(I_x^2 + I_y^2)^{\frac{3}{2}}} \tag{2}$$

This operator is the basis of the well-known corner operator "Kitchen-Rosenfeld" (Kitchen and Rosenfeld, 1982) which is formed by the multiplication of the curvature of isophotes lines and the norm of the gradient. This formula means that a corner point must be an edge point with a strong curvature. Then the Eq. 3:

$$KR = \frac{I_y^2 I_{xx} - 2I_x I_y I_{xy} + I_x^2 I_{yy}}{(I_x^2 + I_y^2)^2} \tag{3}$$

It is also well-known that the Laplacian operator applied to an image can be written as Eq. 4:

$$\Delta I = \frac{I_y^2 I_{xx} - 2I_x I_y I_{xy} + I_x^2 I_{yy}}{(I_x^2 + I_y^2)^2} + \frac{I_x^2 I_{xx} + 2I_x I_y I_{xy} + I_y^2 I_{yy}}{(I_x^2 + I_y^2)^2} \tag{4}$$

Then as Eq. 5 :

$$\Delta I = I_{xx} + I_{yy} = I_{\xi\xi} + I_{\eta\eta} \tag{5}$$

It comes that $I_{\xi\xi}$ is the second derivative of the image along the direction of the isophote ξ and $I_{\eta\eta}$ is the second derivative of the image along the direction of the gradient η. As evidence, KR is equivalent to $I_{\xi\xi}$. The Harris and Stephen (Harris and Stephens, 1988) proposed corner operator based on the structure tensor as Eq. 6;

$$T = \begin{pmatrix} (I_x^2) * G_{\sigma_s} & (I_x I_y) * G_{\sigma_s} \\ (I_x I_y) * G_{\sigma_s} & (I_y^2) * G_{\sigma_s} \end{pmatrix} \tag{6}$$

This structure tensor obtained from gradient tensor represents the local auto-correlation of the image signal. I_x and Y_y are image derivatives along respectively X and Y axis. They are obtained using a Gaussian derivative filter with a σ_d standard-deviation.
G_{σ_s} is a Gaussian smoothing filter with a σ_s standard-deviation.
Then the Harris operator is obtained from this tensor as Eq. 7:

$$H = \mathrm{Det}(T) - k \cdot \mathrm{Trace}(T)^2 \tag{7}$$

- The determinant is the product of eigen values, it is strong when both eigen values are strong.
- The trace is the sum of eigen values and is strong at edges.
- The parameter k has been determined empirically to do a balance between corners and edges. k is generally set to 0.04.

2.1 Diffusion scheme

There are two important diffusion schemes.

- The Euclidean linear scale space :
  This diffusion scheme is described by the Heat equation, whose solution is a convolution of the original image with a Gaussian. Then the Kitchen-Rosenfeld operator can be seen as the curvature multiplied by the gradient at a certain level of diffusion.
- The Euclidean morphological scale space :
  This non-linear scale-space is obtained by applying the Mean Curvature Motion (MCM) scheme (Franke et al., 1996) Eq. 8.

$$\begin{cases} I(0,x,y) &= I_0(x,y) \\ \frac{\partial I}{\partial t}(t,x,y) &= I_{\xi\xi}(t,x,y) \end{cases} \tag{8}$$

  Where ξ still represent the tangent to isophotes. When iterating this scheme, isophote lines are moving in function of their Euclidean curvature. The Fig. 1 illustrates this property. If iterations goes on, the rectangle will be changed to a circle of decreasing radius.

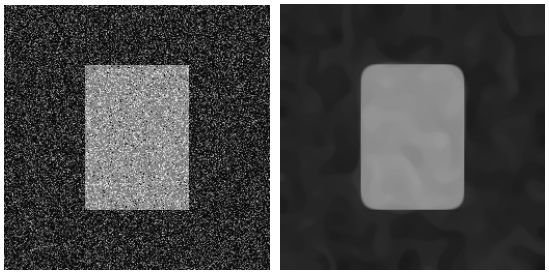

(a) Initial image (b) MCM diffusion

Figure 1: MCM behavior. a) initial image, b) result of MCM diffusion (100 iterations).

It is clear that such diffusion schemes are moving in the corners as well as Gaussian scale space. In both schemes, the $I_{\xi\xi}$ term is present.

3 PROPOSED METHOD

In this study we have used a completely different scheme based on asymmetric diffusion ((Montesinos and Magnier, 2017)) which corresponds exactly to our

needs of detecting corners precisely. Then we are going to show that one curvature-like measure that is used to drive the numerical scheme provides a better alternative to the $I_{\xi\xi}$ operator for corner detection.

3.1 An asymmetric diffusion scheme

At each pixel P, five distinct directions are defined:

- ξ_1 and ξ_2 are the direction defined by the application of a bank of first derivative causal filters. These directions are the direction given by the smoothing component of the filter giving the external response (ξ_1 corresponds to the maximal positive response, ξ_2 to the minimal negative one).
- ξ is the orientation of the tangent to the isophote. This orientation is computed using ξ_1 and ξ_2.
- ξ_{1r} and ξ_{2r} are the mirrored orientations of ξ_1 and ξ_2 by the axis ξ (See Fig. 2a)).

This scheme can then be written as Eq. 9:

$$\left\{ \begin{array}{lll} I(0,x,y) & = I_0(x,y) & \leftarrow \text{ initial image} \\ \frac{\partial I}{\partial t}(t,x,y) & = I_{\hat{\xi_1}\hat{\xi_2}}(t,x,y) = \underset{I_{\xi_1\xi_2}, I_{\xi_{1r}\xi_{2r}}, I_{\xi\xi}}{\arg\min} & |x| \end{array} \right. \tag{9}$$

This scheme has a geometrical interpretation, illustrated at the Fig. 2. We have already seen that orientations ξ_1 and ξ_2 are influenced by the presence of edges, then at each pixel, we are searching for the directions that are the less influenced by edges in order to preserve these edges at most as possible by asymmetric diffusion. The diffusion will be achieved along ξ, along ξ_1 and ξ_2, or along ξ_{1r} and ξ_{2r}, in respect to the minimum absolute value of the asymmetric second derivative of the image. In the configuration of Fig 2b), or Fig. 2c) the diffusion is applied in the direction ξ_{1r} and ξ_{2r}, preserving the edges. On the configuration of Fig. 2a), the pixel under consideration is located on an edge, the diffusion may be either along ξ_1 and ξ_2 or simply along, ξ depending on the local curvature. For this scheme, the only parameter is the number of iterations.

For regularizing the input image, we just proceed to several iterations of this asymmetric scheme (in general, 100 iterations give good results). The Fig. 3 presents results of regularization obtained on the "rectangle image" a), 3b) presents results obtained with 100 iterations, 200 iterations at c) and 500 iterations at d). As we can see, corners are not affected even with a high number of iterations.

3.2 Asymmetric curvature

This scheme uses three curvature-like expressions to perform the diffusion :

- $|I_{\xi_1\xi_2}|$:
  a corner point is first an edge point with a smallest value of $|I_{\xi_1\xi_2}|$ under a certain neighborhood because ξ_1 and ξ_2 are both directions of isophotes then, at the corner point location, the three gray-levels involved in $|I_{\xi_1\xi_2}|$ are similar.
- $|I_{\xi\xi}|$:
  this measure is similar to the Kitchen-Rosenfeld measure (direction ξ may be somewhat different because filters involved are different) estimated locally in a 3×3 window. This measure is suitable but not optimal, the next measure will be preferred.
- $|I_{\xi_{1r}\xi_{2r}}|$:
  this measure is maximized since the directions, ξ_{1r} and ξ_{2r} indicates the directions where gray-levels are the most different from the considered pixel. For this reason, the response obtained is less noisy than the one obtained with the preceding measure.

Then, for characterizing the curvature at corner points, we have chosen to use the expression $|I_{\xi_{1r}\xi_{2r}}|$ that best characterizes the corners. The Fig. 4 presents the three asymmetric curvature results obtained after 100 iterations. As explained beforehand, the $|I_{\xi_1\xi_2}|$ (Fig. 4a)) gives 2 responses at each side of corners. This measure is minimum at corner points, for this reason it will be complicated to use such measure to characterize correctly corners. The $|I_{\xi\xi}|$ (Fig. 4b)) is similar to a Kitchen Rosenfeld measure, the response is overall noisy and edges are also responding. Finally, the $|I_{\xi_{1r}\xi_{2r}}|$ (Fig. 4c) measure gives the best information able to characterize reliably the corner points.

3.3 Corner detection using $|I_{\xi_{1r}\xi_{2r}}|$

The complete algorithm for asymmetric corner detection is summarized as follows :

1. Depending on the precision needed, magnify or not the initial image ((Montesinos and Datteny, 1997)) using a very small Gaussian standard-deviation ($\sigma \simeq 0.6$), apply several iterations (in general 10) of a heat inverse equation scheme then apply several iterations (in general 4) of a shock filter ((Osher and Rudin, 1990)).
2. Apply several iterations of the asymmetric scheme (in general 100).
3. Compute the $|I_{\xi_{1r}\xi_{2r}}|$ image after the regularization.
4. Compute the local maxima of the $|I_{\xi_{1r}\xi_{2r}}|$ for example in a circular window (generally with a radius of 2 pixels multiplied by the precision).

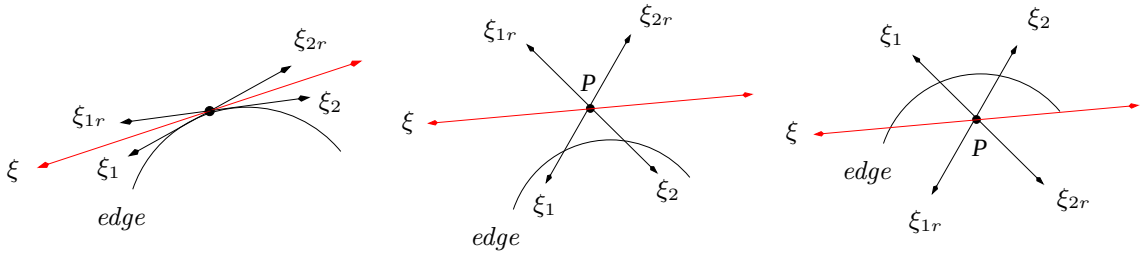

(a) Pixel located on an edge (b) Pixel located outside edge (c) Pixel located inside edge

Figure 2: Causal Orientation. a) The pixel is located on an edge, the diffusion may be either along ξ_1 and ξ_2, b) Pixel is outside edge and the diffusion is applied in the direction ξ_{1r} and ξ_{2r}, preserving the edges, c) Pixel is inside edge and the diffusion is applied in the direction ξ_{1r} and ξ_{2r}, preserving the edges

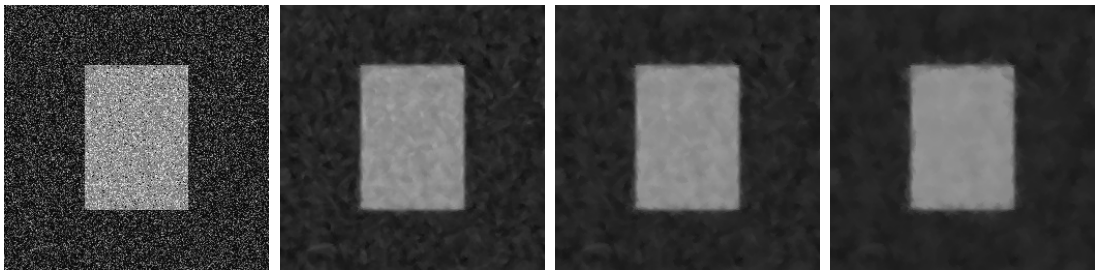

(a) Initial image (b) Regularization 100 iterations (c) Regularization 200 iterations (d) Regularization 500 iterations

Figure 3: Asymmetric regularization. a) initial image, b) asymmetric regularization 100 iterations, c) asymmetric regularization 200 iterations, d) asymmetric regularization 500 iterations.

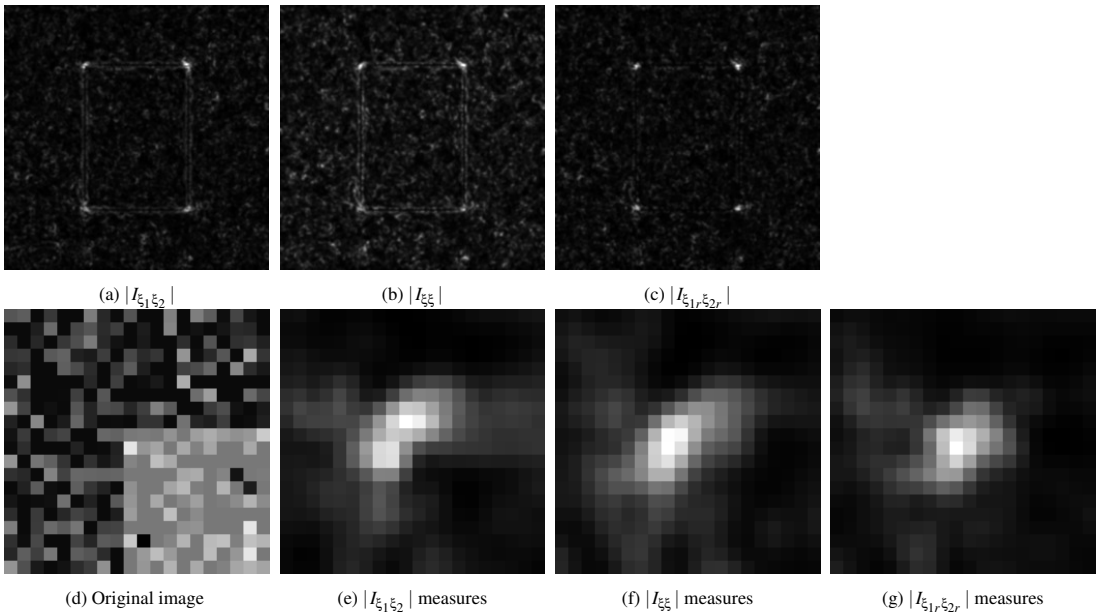

(a) $|I_{\xi_1\xi_2}|$ (b) $|I_{\xi\xi}|$ (c) $|I_{\xi_{1r}\xi_{2r}}|$

(d) Original image (e) $|I_{\xi_1\xi_2}|$ measures (f) $|I_{\xi\xi}|$ measures (g) $|I_{\xi_{1r}\xi_{2r}}|$ measures

Figure 4: Anisotropic curvature measures obtained after 100 iterations. a) $|I_{\xi_1\xi_2}|$, b) $|I_{\xi\xi}|$, c) $|I_{\xi_{1r}\xi_{2r}}|$. d), e), f), g) Details in the upper left corner (d) original image) e, f, g) respectively $|I_{\xi_1\xi_2}|$, $|I_{\xi\xi}|$, and $|I_{\xi_{1r}\xi_{2r}}|$ measures.

4 RESULT

The Fig.5 presents the $|I_{\xi_{1r}\xi_{2r}}|$ operator results obtained on the "rectangle" image at simple pixel precision, after varying number of iterations (100, 200, 500). As iterations go on, the noise is filtered. For comparison, the Fig. 6 presents the Kitchen-Rosenfeld operator results obtained with a Gaussian standard-deviation $\sigma = 1$ and $\sigma = 3$. The Kitchen-Rosenfeld operator gives noisy results. When computed with a Gaussian filter having a parameter σ equal to 1 the results obtained are generally too noisy to obtain interesting results (Fig. 6b)). If the parameter σ increases, it is possible to obtain a more reliable information, but local maxima are moving (Fig. 6c)).

Finally, the Fig. 7 present results obtained by local maxima extraction for all operators : Harris ($\sigma = 1$), Kitchen-Rosenfeld ($\sigma = 3$) and $|I_{\xi_{1r}\xi_{2r}}|$ with 100, 200 and 500 iterations. As discussed beforehand, Harris and Kitchen-Rosenfeld give noisy results. Moreover, for Kitchen-Rosenfeld, corners are often detected at a distance greater than 2 pixels from the true location. Increasing the Gaussian parameter σ improves the curvature SNR (signal-to-noise ratio), but precision of corner localization decreases. Concerning the $|I_{\xi_{1r}\xi_{2r}}|$ operator, the response is less noisy, and the precision seems better than Harris (around 1 pixel from the true corner locations).

The Fig. 8 compares the Harris operator and the anisotropic curvature operator on the "inria" image : a) shows the initial image, b) presents regularization results (100 iterations) and c) presents the $|I_{\xi_{1r}\xi_{2r}}|$ operator result. The Fig. 8 b) and c) show respectively the results of the Harris corner detector and the $|I_{\xi_{1r}\xi_{2r}}|$ corner detection. Then the Fig. 8 d) present 4 manually corner selection and the results obtained with both operators are going to be detailed in Fig. 8 e). For the Fig. 8 e), for those corner angle which is less or equal to 90°, the new operator performs better than Harris, and for those corner angle which is 108° (angle is wider) the results are similar. But if angle value increases Harris completely lost the corner point, The new operator still performs correctly (see the wide angles of the black carpet corners on the floor).

4.1 Sub-pixel precision

The Fig. 9 compares Harris corner detector (threshold=0.001) and $|I_{\xi_{1r}\xi_{2r}}|$ corner detection (threshold=0.05) at pixel precision. We are interested here on the results obtained on the small windows of the central house (windows size is around 5×5 pixels). Harris operator (Fig. 9 b)) gives many responses on the windows, but the points detected are often on the windows frame rather than the corner. For the $|I_{\xi_{1r}\xi_{2r}}|$ (Fig. 9 c)) corner detection, the detected point is more often at the corner. On the large, dark windows of the left house, Harris performs better.

The Fig. 10 present results obtained at precision=2 ($\frac{1}{2}$ pixel). In 10 a) are presented the sub-pixel ($\frac{1}{2}$ pixel) Harris corner detector, and in 10 b) are presented the sub-pixel ($\frac{1}{2}$ pixel) $|I_{\xi_{1r}\xi_{2r}}|$ corner detector. The Fig. 10 c) and d) present the details only a region of interest 200×200 on the windows of the central house (c) Harris, d) $|I_{\xi_{1r}\xi_{2r}}|$.

5 CONCLUSIONS

This paper presents an asymmetric diffusion-based anisotropic causal corner operator. The proposed approach presented higher precision and accuracy than the compared well-known corner detectors, such as Kitchen Rosenfeld and Harris and Stephen techniques, which are known as a reference benchmarks. Meanwhile, to better regularize the image and improve the robustness against noises, an asymmetric diffusion scheme is used. The experimental results on synthetic images and real images, both on pixel and subpixel precision, validate visually the performance of our method. This work can particularly contribute to applications that require keypoint detection with higher precision, such as 3D reconstruction (Peng et al., 2009), object detection, etc. Correspondingly, as the outlook of this work will be to examine this technique for the 3D reconstruction and then pursue an objective evaluation (Shokouh et al., 2023).

REFERENCES

Franke, T., Neumann, H., and Seydel, R. (1996). Anisotropic diffusion based on mean curvature motion: A computational study. In Jähne, B., Geißler, P., Haußecker, H., and Hering, F., editors, *Mustererkennung 1996*, pages 47–54, Berlin, Heidelberg. Springer Berlin Heidelberg.

Harris, C. G. and Stephens, M. J. (1988). A combined corner and edge detector. In *Alvey Vision Conference*, pages 147–151.

Junfeng, J., Shenjuan, L., Gang, W., Weichuan, Z., and Changming, S. (2022). Recent advances on image edge detection: A comprehensive review. *Neurocomputing*.

Kitchen, L. and Rosenfeld, A. (1982). Gray-level corner detection. *Pattern Recognit. Letters*, 1:95–102.

Montesinos, P. and Datteny, S. (1997). Sub-pixel accuracy using recursive filtering. In *Scandinavian Conference on Image Analysis*.

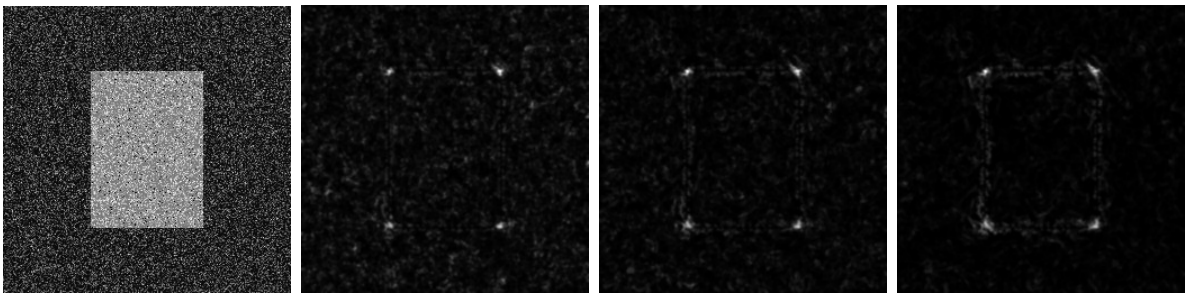

(a) Original image (b) $|I_{\xi_{1r}\xi_{2r}}|$ at 100 iterations (c) $|I_{\xi_{1r}\xi_{2r}}|$ at 200 iterations (d) $|I_{\xi_{1r}\xi_{2r}}|$ at 500 iterations

Figure 5: Asymmetric curvature $|I_{\xi_{1r}\xi_{2r}}|$ on image "rectangle". a) original image, b) $|I_{\xi_{1r}\xi_{2r}}|$ at 100 iterations, c) $|I_{\xi_{1r}\xi_{2r}}|$ at 200 iterations, d) $|I_{\xi_{1r}\xi_{2r}}|$ at 500 iterations.

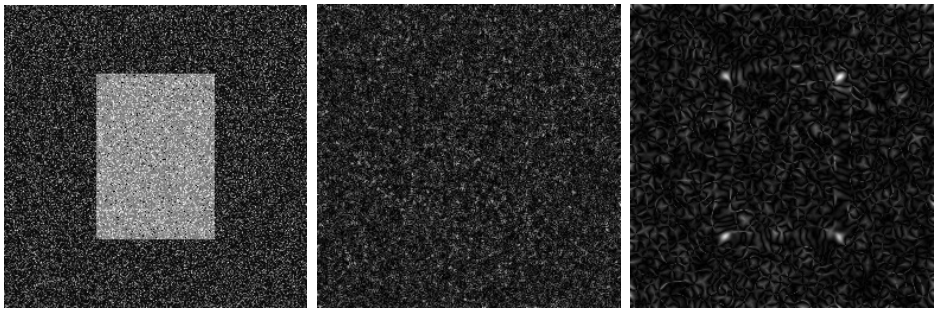

(a) Original image (b) Kitchen-Rosenfeld ($\sigma = 1$) (c)Kitchen-Rosenfeld ($\sigma = 3$)

Figure 6: Kitchen-Rosenfeld operator on image "rectangle". a) original image, b) Kitchen-Rosenfeld ($\sigma = 1$) regularization is not enough to obtain reliable curvature, c) Kitchen-Rosenfeld ($\sigma = 3$) curvature appears, but noise is still present and strong.

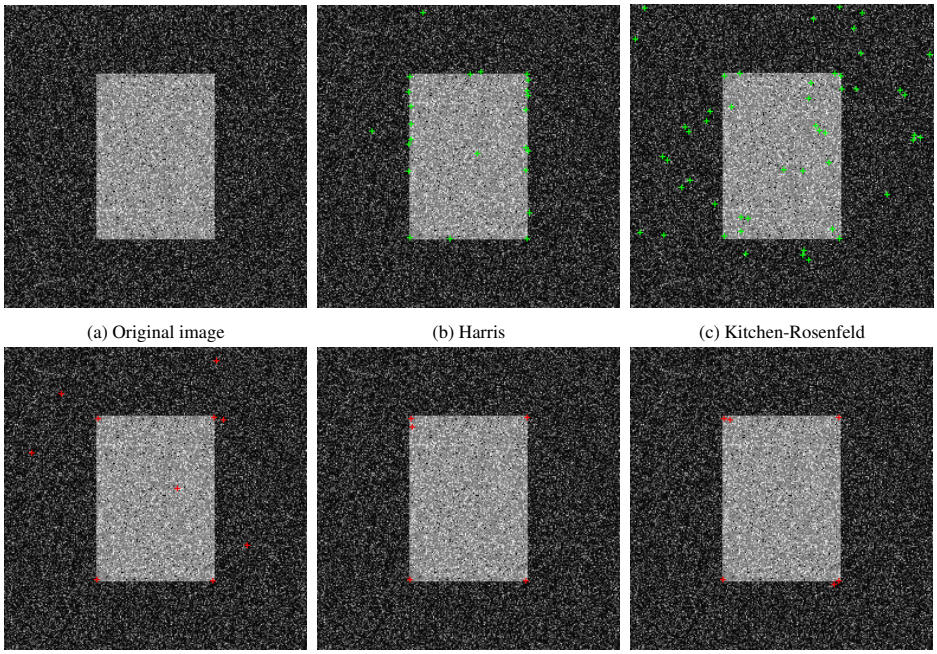

(a) Original image (b) Harris (c) Kitchen-Rosenfeld

(d) Anisotropic (100 iteration) (e) Anisotropic (200 iteration) (f) Anisotropic (500 iteration)

Figure 7: Corner detection. a) Harris corner detector (threshold = 0.1), b) Kitchen-Rosenfeld corner detector ($\sigma = 3$, threshold=0.3), c) Anisotropic corner detector (100 iterations, threshold = 0.3), d) Anisotropic corner detector (200 iterations, threshold = 0.3), e) Anisotropic corner detector (500 iterations, threshold = 0.3.

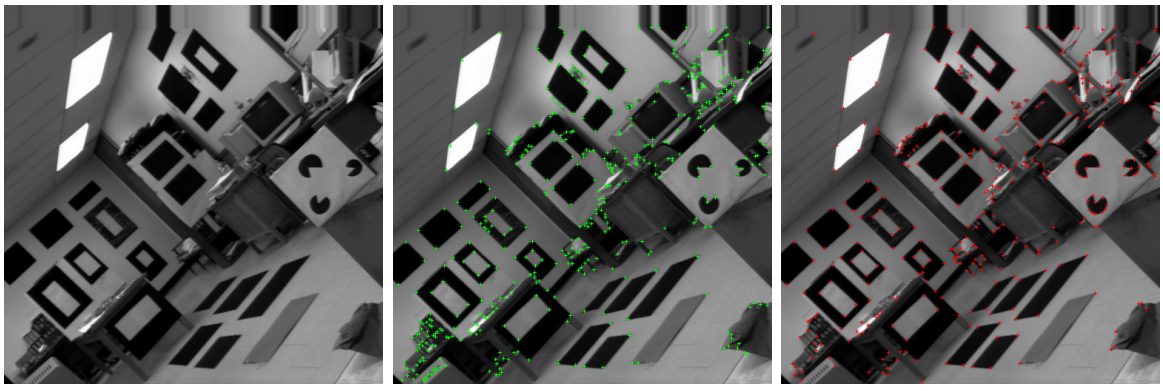

(a) Original image (b) Harris (c) Proposed anisotropic

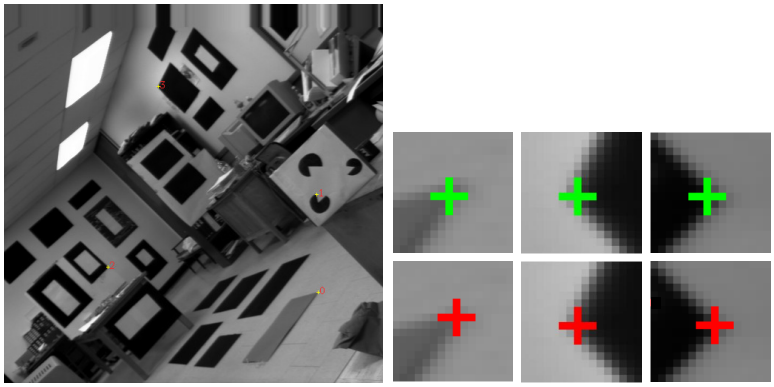

(d) Corner locations highlighted (e) Corner (424, 390),(209, 112), (140, 355) of d

Figure 8: *Corner detection on the image "inria". a) Original image, b) Harris corner detection operator (threshold = 0.001) , c) Anisotropic corner detection operator (threshold = 0.1). d) Few detected corner highlighted. e) Comparative corner precision at location(424, 390),(209, 112), (140, 355) highlighted in d)*

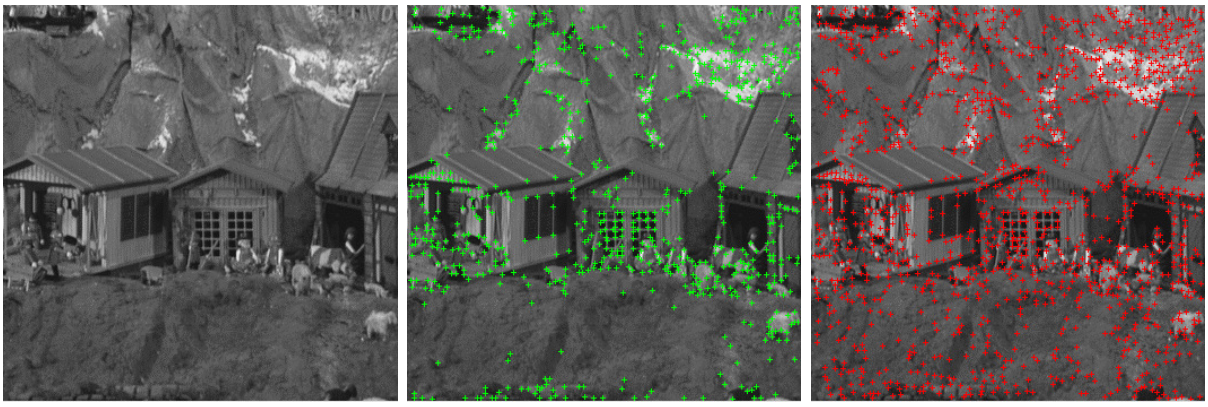

(a) Initial image (b) Harris (c) Proposed anisotropic

Figure 9: Corner detection image "toys", pixel precision. a) initial image. b) Harris corner detector (threshold = 0.001), c) Anisotropic corner detector (threshold = 0.05).

Montesinos, P. and Magnier, B. (2017). Des filtres anisotropes causaux pour une diffusion non controlled. In *GRETSI*.

Osher, S. and Rudin, L. (1990). Feature-oriented image enhancement using shock filter. In *SIAM Journal of Numerical Analysis*.

Peng, K., Chen, X., Zhou, D., and Liu, Y. (2009). 3d reconstruction based on sift and harris feature points. In *2009 IEEE International Conference on Robotics and Biomimetics (ROBIO)*, pages 960–964.

Schmid, C., Mohr, R., and Bauckhage, C. (2010). Evaluation of interest point detectors. *IJCV*, 37:151–172.

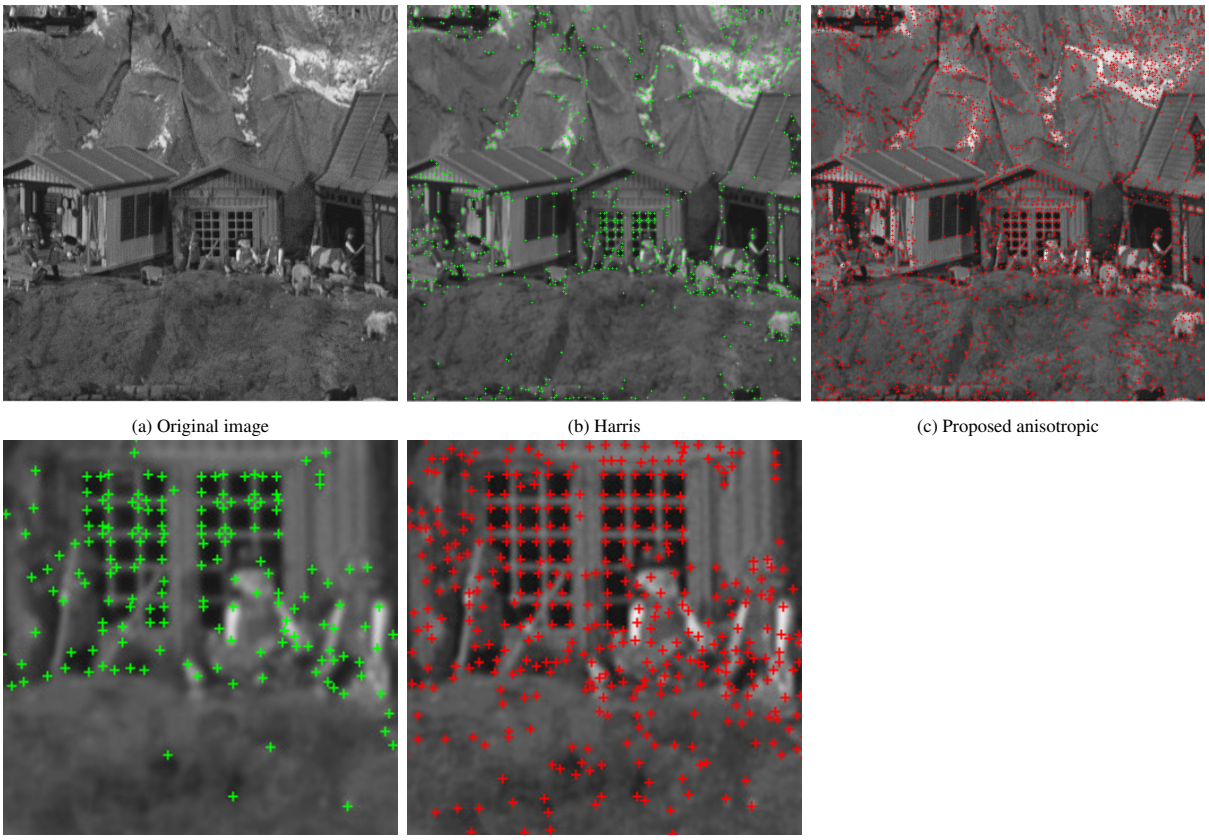

(a) Original image (b) Harris (c) Proposed anisotropic

(d) Harris (window details) (e) Proposed (window details)

Figure 10: Corner detection image ”toys”, precision = $\frac{1}{2}$ pixel. a) Harris corner detector (threshold = 0.001), b) Anisotropic corner detector (threshold = 0.05), c) Harris corner detector (window details), d) Anisotropic corner detector (window details).

Shokouh, G.-S., Montesinos, P., and Magnier, B. (2023). Repeatability evaluation of keypoint detection techniques in tracking underwater video frames. In *CVAUI, to appear*. Springer Berlin Heidelberg.

Wang, L., Han, K., and Sun, H. (2019). An adaptive corner detection method based on deep learning. In *2019 Chinese Control Conference (CCC)*, pages 8478–8482.